Journal of Thermal Analysis and Calorimetry, Vol. 88 (2007) 1, 127–132

SOLID STATE REACTIONS IN THE PLATINUM–MERCURY SYSTEM
Thermogravimetry and differential scanning calorimetry

G. R. Souza[1], *I. A. Pastre*[2], *A. V. Benedetti*[1], *C. A. Ribeiro*[1] *and F. L. Fertonani*[1]*

[1]DQA – Instituto de Química, Unesp, Araraquara, São Paulo, C.P. 355, CEP 14.801-900, Brazil
[2]DQCA-IBILCE-Unesp, S. J. Rio Preto, Brazil

Thermogravimetry, Differential Scanning Calorimetry and other analytical techniques (Energy Dispersive X-ray Analysis; Scanning Electron Microscopy; Mapping Surface; X-ray Diffraction; Inductively Coupled Plasma Atomic Emission Spectroscopy and Cold Vapor Generation Atomic Absorption Spectroscopy) have been used to study the reaction of mercury with platinum foils. The results suggest that, when heated, the electrodeposited Hg film reacts with Pt to form intermetallic compounds each having a different stability, indicated by at least three mass loss steps. Intermetallic compounds such as $PtHg_4$, PtHg and $PtHg_2$ were characterized by XRD. These intermetallic compounds were the main products formed on the surface of the samples after partial removal of bulk mercury via thermal desorption. The Pt(Hg) solid solution formation caused great surface instability, attributed to the atomic size factor between Hg and Pt, facilitating the acid solution's attack to the surface.

Keywords: *DSC, intermetallic compounds, mercury, platinum, TG, XRD*

Introduction

The existence of mercury in the atmosphere and troposphere as a pollutant promotes the contamination of many different materials and makes a great number of chemical and electrochemical processes possible. Mercury contamination of noble metals and their alloys can also invalidate their use. For example, when being used as a standard mass reference material or as an electrical contact in an electrical and electronic devices due to the new intermetallic species and oxides formed [1–3]. Pt, Rh, Ir and their alloys have many technological applications, for instance, as catalysts in the petroleum cracking industry; as catalysts supported on alumina [4] or on SiC; as catalyst support in exhaust catalyst sources [5]; on SiO_2 and TiO_2 in automotive exhaust gas oxidation of NO to NO_2 and SO_2 to SO_3 [6, 7]; as a chemical catalyst material in ammonia oxidation plants [8], and in many other electrical devices [1]; as microelectrodes and ultramicroelectrodes in electrochemistry [9, 10]. Mercury easily interacts with these noble metals and their alloys [3, 11–26], which can be an advantage or a disadvantage depending on the application of the resulting material. Also, as mercury can be present in petroleum as a contaminant, some problems appear mainly due to the formation of solid intermetallic compounds, since they can modify the catalytic properties in the petroleum cracking process. On the other hand, platinum, mercury and other metals can be electrodeposited on conductive thin-film diamond surfaces to produce novel catalytic electrodes, sensors and detectors [1].

Recently, solid-state reactions of mercury with Pt, Rh and Ir, along with some alloys, namely Pt–Ir (20 mass%), Pt–Rh (10 mass%), Pt–Ir (30 mass%) were studied using different techniques [11, 17, 18, 22–26]. The results allowed us to suggest that the electrodeposited mercury film, when heated, reacts with Pt, Pt–Rh (10 mass%) and Pt–Ir (20 mass%) alloys to form products having different stabilities, indicated by more than one mass loss step. These mass loss steps were associated to the following factors: bulk Hg removal, monolayer mercury desorption, thermal decomposition of intermetallic compounds and mercury removal from a solid solution of Pt and Pt–Ir alloy containing mercury.

In the present work, mercury films were electrodeposited on platinum foils and the unreacted mercury was removed by thermal desorption, as described previously [11, 17, 18]. At the end of each step of the thermal mercury removal, the sample surface was examined using X-ray diffractometry (XRD), scanning electron microscopy (SEM), energy dispersive X-ray microanalysis (EDX), atomic absorption and emission spectrometry. These techniques allowed us to characterize in detail the nature of the intermetallic phases formed on the surface of platinum-mercury system.

* Author for correspondence: fertonan@iq.unesp.br

1388–6150/$20.00

Akadémiai Kiadó, Budapest, Hungary
Springer, Dordrecht, The Netherlands

Experimental

Preparation and pre-treatment of Pt foils (Heraeus Vectra, 99.99% (mass/mass)) quenched from 1200 to 0°C, and Hg electrodeposition were carried out under the following conditions: $E_{deposition}$= – 0.35V/Ag|AgCl|$KNO_{3(sat.)}$, $t_{deposition}$=300 s using $60.0 \cdot 10^{-3}$ mol L^{-1} Hg(I) unstirred solution, followed by Hg thermal removal and chemical analysis of Hg and Pt as previously described [11, 17, 18]. Thermogravimetry (TG) and Differential Scanning Calorimetry (DSC) curves were obtained from 30 to 900ºC and 30 to 600ºC, respectively, at β=5ºC min^{-1}, under a purified N_2 atmosphere flux of about 150 mL min^{-1}, using a TG-50 thermobalance and a DSC-25 calorimeter coupled to a TC-15 processor (Mettler-Toledo, Greifensee, Switzerland). An α-alumina and aluminium crucible with a perforated lid (ϕ=1 mm) were used to obtain the TG and DSC curves, respectively.

The sample surfaces before and after they had been heated up to different temperatures were examined using a JEOL JSM-T330A (JEOL, Ltd. Of Akishima, Japan) microscope with a NORAN EDX (Energy Dispersive X-ray Analysis) (Thermo Electron Corporation Waltham, MA) coupled system in order to take SEM (Scanning Electron Microscopy) images, undertake EDX-microanalysis and do the mapping of the elements, and a D-5000 SIEMENS X-ray diffractometer (Siemens D5000, Karlsruhe, Germany) was implemented to obtain the patterns diffractions.

The data generated from the X-ray diffraction studies were treated using AFPAR software (Complex des Programme, CNRS, France) in order to determine the lattice parameters of any possible intermetallic species which may have formed on Pt foil surface [27]. This method makes use of Experimental Interplanar Spacing (d-spacing), shown in Table 1, where the data are taken from a data base reference such as those for $PtHg_4$ or $RhHg_2$ (lattice parameters and the respective reflection values) [28]. Both of these parameters were put together to obtain the experimental lattice parameters [17, 29]. The resulting experimental parameters ($a \pm \sigma$), ($b \pm \sigma$), ($c \pm \sigma$) are individually presented in Table 2, compared with the respective data-base reference parameters. Mercury content was analyzed by atomic absorption spectroscopy using the cold-vapor steam-generation technique and an INTRALAB-VARIAN, AA/1475 spectrometer, while platinum was analyzed by ICP using an ICP-AES (Sequential Espectroflame) spectrometer [17].

Results and discussion

Figures 1 and 2 show the TG/DTG and DSC curves for the quenched platinum-mercury system, respectively. The TG curve (Fig. 1a) depicts mass losses in three consecutive steps between 30 and 400°C, although the DTG curve (Fig. 1b) showed only two steps clearly. The last step of TG curve is a small one and it is better visualized from the detail inserted in Fig. 1a. On the other hand, the DSC curve (Fig. 2)

Table 1 XRD experimental data obtained for the quenched Pt foil surface heating up to T=147°C and T=240°C; β: 5°C min^{-1}; N_2 flow rate: 150 mL min^{-1}. $K\alpha_{Cu}$: 1.54184 Å

2θ	Int./%	$d_{exp.}$	$d_{tab.}$*	*h k l*	Compound
			T=147°C		
20.35	13	4.375	4.369	0 1 1	$PtHg_4$
28.90	77	3.089	3.090	0 0 2	$PtHg_4$
32.25	12	2.773	2.764	0 1 2	$PtHg_4$
35.55	17	2.525	2.523	1 1 2	$PtHg_4$
41.30	100	2.183	2.185	0 2 2	$PtHg_4$
51.10	15	1.787	1.784	2 2 2	$PtHg_4$
59.75	33	1.548	1.545	0 0 4	$PtHg_4$
67.75	17	1.383	1.382	0 2 4	$PtHg_4$
			T=240°C		
26.60	100	3.351	3.349	1 1 0	$PtHg_4$
39.35	39	2.290	2.280	0 2 2	Pt_3O_4
39.65	16	2.273	2.267	0 2 0	PtO_2
41.30	2	2.187	2.186	1 1 1	$PtHg_2$
48.90	14	1.912	1.901	1 2 2	Pt_3O_4
54.80	7	1.675	1.674	2 2 0	$PtHg_2$

*obtained from [28]

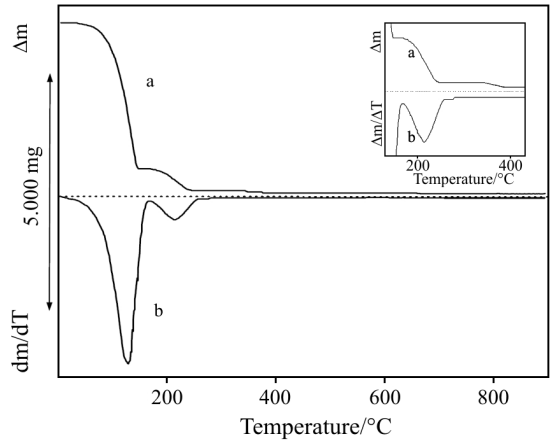

Fig. 1 a – TG and b – DTG curves for quenched Pt foil containing electrodeposited Hg; β=5°C min^{-1}; N_2 flux: 150 cm^3 min^{-1}. Inserted detail: magnification of 2nd and last mass loss step

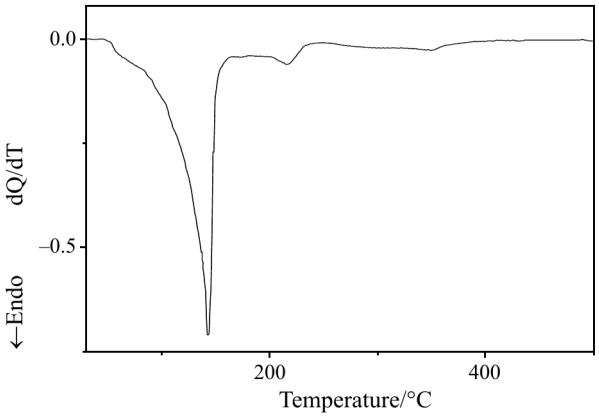

Fig. 2 DSC curves for quenched Pt foil containing electrodeposited Hg; β=5°C min^{-1}; N_2 flux: 150 cm^3 min^{-1}

shows three endothermic peaks, which occurred at 143, 217 and 350°C. These peaks are in agreement with the TG-curve steps and the endothermic peak at 350°C allowed us to confirm the existence of the third step of TG curve. The first mass-loss step, from 30 to 147°C in TG/DTG curves, occurs as a very rapid process and can be attributed to the loss of electrodeposited mercury bulk in agreement with the results already described [11, 16, 19, 22, 25, 26]. The quantity of mercury lost in this step corresponds to 80% of the total electrodeposited mercury. This mercury content completely 'wet' the foil surface because mercury has a lower mercury-substrate contact angle.

The DSC curve (Fig. 2) shows only endothermic peaks at 143, 217 and 350°C, as previously described, which correspond to the mass-loss steps observed in the TG curve. The endothermic peak at 143°C was ascribed to the mercury bulk removal.

Figure 3a shows the SEM image of the Pt foil surface covered with a film of $PtHg_4$ intermetallic species identified by the XRD (Tables 1 and 2). Figures 3b and c respectively show the Pt and Hg mappings obtained on the platinum surface after mercury bulk removal occurred by heating the system up to 147°C. This is the temperature which corresponds to the end of the first mass loss step in the TG curves. The SEM image shows a rough surface covered by a homogeneous solid-gray film. In a parallel experiment, the heating process (β=5°C min^{-1}) was stopped at 110°C and then the sample was cooled to room temperature.

A solid-gray material having a characteristic aspect similar to $PtHg_4$ was observed on the platinum surface in agreement with that previously described [20, 22]. The solubility of Pt increases in bulk mercury from 0.202 at. % at 70°C to 0.910 at. % at 110°C [12]. X-ray diffractometry results for a platinum surface heated up to 147°C are shown in Tables 1 and 2 and indicate that $PtHg_4$ (cubic: a=(6.17±0.01) Å) is the most probable intermetallic compound formed.

For atomic emission analysis, the platinum foil surfaces heated up to 147°C were attacked with acid solutions (concentrated HNO_3 in the presence of three drops of concentrated HCl) as already described [17, 11]. It is interesting to note that for Pt–Hg systems such as Pt–Rh(10 mass%), Pt–Ir(20 mass%) and Pt–Ir(30 mass%) [11, 18, 25], platinum was also detected in the resultant solution (Table 3). These results clearly demonstrated the instability of the Pt surface and this can be ascribed to a Pt–Hg interaction. This seems to indicate that the atomic-size factor be-

Table 2 Comparison between calculated crystalline lattice parameters from the Pt–Hg system using the experimental data from Table 1 and the data-base reference parameters of similar systems

Reference material	System	$a^*_{(experimental)}$	$c^*_{(experimental)}$	Error/%
$PtHg_4$	Pt–Hg			
T=147°C				
a=6.1808±0.0004**		6.176±0.006	–	a, 0.07
$PtHg_2$	Pt–Hg			
T=240°C				
a=4.675±0.002**		4.666±0.005	–	a, 0.5
c=2.918±0.001**			2.9132±0.0028	c, 0.2

*obtained from [28], **calculated using previously referenced software programs [27]

tween Hg and Pt introduces a surface destructuring which facilitates the attack of the Pt surface by the acid solution [11, 17, 18, 22].

The second TG step observed between 147 and 240°C was ascribed to the thermal decomposition of the intermetallic $PtHg_4$ film (Tables 1 and 2) as already observed [16, 18, 19, 21, 22, 25]. For this temperature range, the mass loss was about 18.1% of the total electrodeposited mercury. The presence of mercury on the platinum surface at the end of this step (T=240°C) was confirmed using EDX microanalysis (Fig. 4a) and flameless atomic absorption (AA-Flameless) (Table 3). The DSC curve (Fig. 2) shows a narrow region of temperature stability from 160 to 200°C after a low intensity endothermic peak at 217°C and bulk mercury removal had occurred. This peak was ascribed to the thermal decomposition of the stable $PtHg_4$ intermetallic compound in agreement with the TG-DTG curves and the XRD data (Tables 1 and 2).

The $PtHg_2$ intermetallic compound (tetragonal: a=4.666±0.005 Å) (Tables 1 and 2) was also identified by XRD at the end of the second step (T=240°C), but not at the end of the first mass-loss step (147°C). Therefore, the origin of $PtHg_2$ can be explained as follows: In this system, $PtHg_2$ did not originate from the decomposition of $PtHg_4$ (reaction 1) as observed for Pt–Rh(10 mass%) and Pt–Ir(30 mass%) alloys [22, 25] since $PtHg_2$ is not stable in the absence of the isostructural $RhHg_2$ compound and is only detected when produced by the decomposition of PtHg via an eutectoide reaction (reaction 2).

Table 3 Atomic absorption flameless (AA-Flameless) and atomic emission (AES-ICP) data for Hg and Pt after partial or total elimination of the mercury by heating up to the specified temperatures

Material	T/°C	m_i/mg	m(Hg)/mg*	m(Pt)/mg**
Pt	147	15.756	0.509	0.310
Pt	240	17.263	0.0779	0.674
Pt	450	17.638	0.0162	0.0979
Pt	800	16.638	–***	–***

*Hg–AA–Flameless ; **Pt–AES-IPC;
***Under detection limits

PtHg and $PtHg_4$ intermetallic compounds are stable as indicated by their presence on Pt–Rh and Pt–Ir alloy interlayers even when they were heated up to 170°C [22, 25]. These results allow us to suggest the presence of a thin PtHg film on the platinum surface under the $PtHg_4$ intermetallic film.

$$PtHg_4 \rightarrow Pt+4Hg \quad (1)$$

$$PtHg \rightarrow PtHg_2 + Pt(Hg)_{solid\ solution} \quad (2)$$

The Pt and Hg mappings and the SEM images obtained for the platinum surface after partial mercury removal by heating up to 240°C and also a temperature corresponding to the end of the second step of the TG curve are shown in Figs 3d, e and f respectively. After

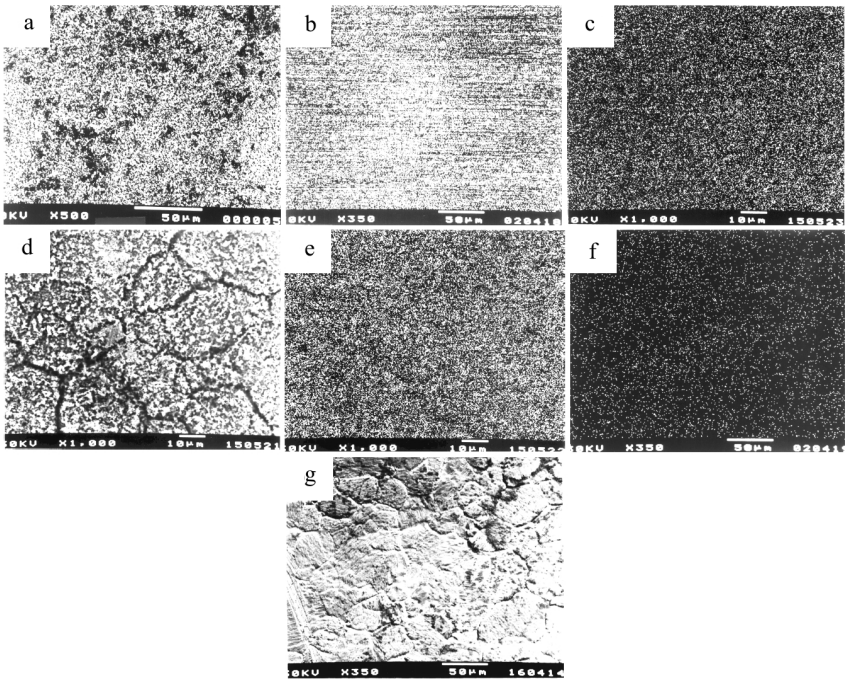

Fig. 3 SEM images and Pt and Hg mappings of quenched Pt foil surface after mercury electrodeposition and heating up to different temperatures: a – SEM, 147°C; b – Pt mapping; c – Hg mapping; d – SEM, 240°C; e – Pt mapping; f – Hg mapping; g – SEM, 900°C. Electron beam acceleration: 30 kV. Magnifications: 350× (b, f, g); 500× (a) and 1000× (c, d, e)

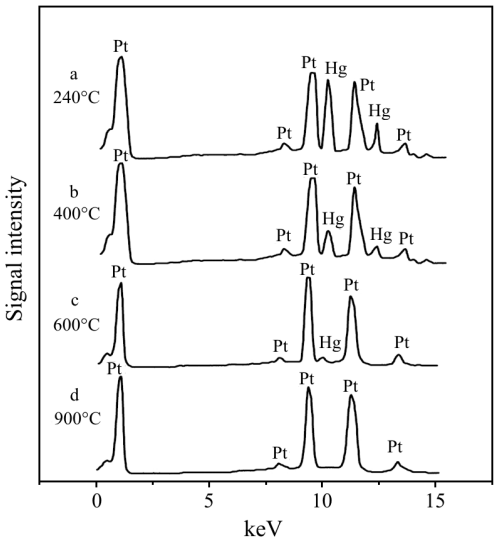

Fig. 4 EDX microanalysis of the surface of quenched Pt foil surface heating up to different temperatures. Sample time: a – 100 s; b – and c – 300 s; d – 500 s. Electron beam acceleration: 30 kV

partial mercury removal (T=240°C) was achieved, well-defined grain boundaries were observed, as shown in Fig. 3d, showing that the surface structure was basically maintained. However, the Pt surface exhibits a morphology (Fig. 3d) which is very different from that shown by Pt–Rh(30 mass%), Pt–Ir(20 mass%) and Pt–Ir(30 mass%) alloys [11, 22, 25].

Mappings of elements, Figs 3e and f, revealed a homogeneous platinum and mercury distribution over the entire foil surface suggesting that a mercury film still exists. The X-ray diffractometry data obtained for the sample at the end of the second step of the TG curve (240°C) allowed us to suggest the existence of the $PtHg_2$ intermetallic compound [22], and the Pt_3O_4 (cubic) and PtO_2 (tetragonal) oxides (Tables 1 and 2). These results are in agreement with the mapping analysis which indicates a homogeneously-distributed mercury film on the surface of the alloy (Fig. 3f) and this was also shown in the EDX microanalysis (Fig. 4a).

The last mass-loss step in the TG curve (Fig. 1a; inset detail) for the Pt-foil system corresponds to a very slow process ranging from ca. 240 to ca. 900°C. This step can be separated into two temperature ranges: a) the first one being from ca. 240 to ca. 450°C (Δm=1.5%) and is ascribed to the thermal decomposition of the $PtHg_2$ compound formed at the end of the second mass-loss step, as previously described; b) the second one is from ca. 450 to ca. 900°C (Δm=0.2%) and is ascribed to the removal of mercury from the subsurface of the platinum substrate [11, 19, 22].

At these different temperature ranges, mercury was detected on the Pt-foil surface when submitted to EDX microanalyses (Figs 4a–c) and chemical analysis (Table 3) even when the samples were heated up to intermediate temperatures (400≤T≤700)°C.

Despite of the differences between the exact temperatures utilized (Fig. 4 and Table 3), these mercury EDX-microanalysis results agree with those obtained by the flameless atomic absorption (AA-Flameless) method (Table 3). Thus, for the platinum substrate, over the entire temperature range from 240 to 900°C, the intensity of the Hg peaks diminish in the EDX microanalysis as the heating temperature increases (Figs 4a to d). At the same time, the Hg content decreases as indicated by the chemical analysis result (Table 3).

It is important to note that mercury was not detected for heating temperatures higher than 800°C (EDX spectrum not shown) while mercury still existed on the surface of Pt–Rh(10 mass%)–Hg [22] and Pt–Ir(20 mass%)–Hg systems [18] at 800°C.

The DSC curve (Fig. 2) shows a low-intensity endothermic peak at 350°C, ascribed to the last step of mercury removal in agreement with the TG curve (Fig. 1a; inset detail). The endothermic signal observed from 250 to 400°C was attributed to the thermal decomposition of $PtHg_2$ and a simultaneous Hg desorption from the subsurface of the platinum foil. Although for the TG curves, Hg desorption from the Pt subsurface can be observed up to 600°C (Fig. 4c).

The SEM surface image (Fig. 3g) obtained after total mercury removal by heating the Pt foil up to 900°C, the temperature corresponding to the end of the last mass-loss step of the TG curves, shows a rearranged surface and suggests a considerably less rough surface. At 900°C, the mercury present in the Pt–Hg amalgam was removed (lower than the detection limit of the EDX microanalysis – Fig. 4d) and the surface was thermally restructured.

A comparison for Pt and Pt–Ir(20 mass%) alloy foils [17] treated at the same temperature range, exhibit: 1) a less rough surface; 2) clearly observed grain boundaries. The X-ray pattern obtained for Pt-foil samples heated up to 450 and 600°C, which is the middle of the last step (not shown in Table I) reveals peaks which can be attributed only to the substrate (Pt) and oxides such as Pt_3O_4 (cubic system) and PtO_2 (tetragonal system). However, at this temperature range, mercury was also detected on the Pt-foil surface by EDX microanalysis (Figs 4b and c) showing the solid solution formation of Pt(Hg) suggesting that Hg diffuses into the lattice restructuring the substrate surface as was also confirmed by atomic absorption flameless (AA-Flameless) analysis (Table 3).

The Pt surface was considerably attacked under specific conditions because mercury has a lower contact angle (Hg-substrate) and completely ‘wet’ the foil surface.

Conclusions

Mercury films electrodeposited on Pt were studied via TG-DTG, DSC and surface analysis to identify the possible formation of intermetallic compounds. The homogeneous mercury film formed on the Pt-foil surface was characterized and the intermetallic compounds ($PtHg_4$, PtHg and $PtHg_2$) were identified on the Pt foil and the formation of amalgam was suggested. The Pt–Hg system lost mercury in at least three steps: 1) from room temperature to 147ºC, only bulk Hg was removed and a $PtHg_4$ film was found covering a film of PtHg; 2) from 147 to 240ºC, the second mass loss occurs and was ascribed to the thermal decomposition of the compound $PtHg_4$; 3) the last mass-loss step from 240 to 900ºC was ascribed to the formation and decomposition of $PtHg_2$ and mercury removal from the Pt(Hg) solid solution. The formation of this solid solution caused a great surface instability, ascribed to the atomic size factor between the Hg and Pt, facilitating the attack of the acid solution on the surface.

The Pt surface was considerably attacked under specific conditions because mercury has a lower contact angle (Hg-substrate) and completely 'wet' the foil surface. The Pt-foil surface obtained after heating up to 900°C shows a reformed surface being considerably less rough and free of mercury.

Acknowledgements

The authors are grateful to CAPES and FUNDUNESP for awarding the fellowship to G. R. de Souza and F. L. Fertonani.

References

1 M. Awada, J. Strojek and G. M. Swain, J. Electrochem. Soc., 142 (1995) 142.
2 K. G. Kreider, M. J. Tarlov and J. P. Cline, Sensor Actuator B-Chem., 289 (1995) 167.
3 P. J. Cumpson and M. P. Seah, Nat. Phys. Lab. (UK), Int. Comm., (1994) 32.
4 R. W. Joyner and E. S. Shpiro, Catal. Let., 9 (1991) 239.
5 M. B. Kizling, P. Stenius, S. Andersson and A. Frestad, Appl. Catal. B-Environ, 1 (1992) 149.
6 E. Xue, K. Seshan, J. G. Vanommen and J. R. H. Ross, Appl. Catal. B-Environ, 2 (1993) 183.
7 G. E. Poirier, B. K. Hance and J. M. White, J. Phys. Chem., 97 (1993) 5965.
8 J. L. G. Fierro, J. M. Palacios and F. Tomas, J. Mater. Sci., 27 (1992) 685.
9 M. Fleishmann, S. Pons, D. Robson and P. P. Schmidt (Eds.), Ultramicroelectrodes, Datatech Science Morganton, N.C., (1987).
10 R. M. Whigtmann and D. O. Wipf, in A. J. Bard (Ed.), Electroanalytical Chemistry, Vol. 15, Marcel Dekker, New York, (1989).
11 F. L. Fertonani, A. V. Benedetti and M. Ionashiro, Thermochim. Acta, 265 (1995) 151.
12 C. Guminski, Bull. Alloy Phase Diagrams, 11 (1990) 26.
13 C. Guminski and Z. Galus. In: C. Hirayama, C. Guminski and Z. Galus, Eds, IUPAC Solubility Data Series: Metals in Mercury, Vol. 25, Pergamon Press, Oxford (1986), p. 330.
14 T. B. Massalski, H. Okamoto, P. R. Subramanian and L. Kacprzak (Eds), Binary Alloy Phase Diagrams, A. S. M. International Press, USA, 3 (1990).
15 S. P. Kounaves and J. Buffle, J. Electroanal. Chem., 216 (1987) 53.
16 S. Affrossman and W. G. Erskine, Trans. Faraday Soc., 62 (1966) 2922.
17 E. Milaré, F. L. Fertonani, M. Ionashiro and A. V. Benedetti, J. Therm. Anal. Cal., 59 (2000) 617.
18 F. L. Fertonani, A. V. Benedetti, J. Servant, J. Portillo and F. Sanz, Thin Solid Films, 341 (1999) 147.
19 S. Affrossman, W. G. Erskine and J. Paton, Trans. Faraday Soc., 64 (1968) 2856.
20 S. K. Lahiri and D. Gupta, J. Appl. Phys., 51 (1980) 5555.
21 G. D. Robbins and C. G. Enke, J. Electroanal. Chem., 23 (1969) 343.
22 E. Y. Ionashiro and F. L. Fertonani, Thermochim. Acta, 383 (2002) 153.
23 E. Milaré, E. Y. Ionashiro, Y. Maniette, A. V. Benedetti and F. L. Fertonani, Port. Electrochim. Acta, 21 (2003) 69.
24 E. Milaré, E. Y. Ionashiro, A. V. Benedetti and F. L. Fertonani, Port. Electrochim. Acta, 21 (2003) 155.
25 E. Milaré, J. R. Turquetti, G. R Souza, A. V. Benedetti and F. L. Fertonani, J. Therm. Anal. Cal., 86 (2006) 403.
26 F. L. Fertonani, E. Milaré, A. V. Benedetti and M. Ionashiro, J. Therm. Anal. Cal., 67 (2002) 403.
27 B. Lestiene and M. Saux, R. VDM., Calcul d'affinement des paramètres cristallins (AFPAR), Complex des Programme, CNRS, France, (1990) Software.
28 Powder Diffraction File PDF2, Data Base Sets 1–44, published by the Jointer Commitee on Powder Diffraction Standard – International Centre for Diffraction Data, Pensylvania, (1988) CD-ROM.
29 A. B. Silva Moitinho, E. Y. Ionashiro, G. R. Souza and F. L. Fertonani. J. Therm. Anal. Cal., 75 (2004) 559.

DOI: 10.1007/s10973-006-8037-9